

# Coulomb breakup effects on the elastic cross section of ${}^6\text{He}+{}^{209}\text{Bi}$ scattering near Coulomb barrier energies

T. Matsumoto,<sup>1,\*</sup> T. Egami,<sup>2</sup> K. Ogata,<sup>2</sup> Y. Iseri,<sup>3</sup> M. Kamimura,<sup>2</sup> and M. Yahiro<sup>2</sup>

<sup>1</sup>*Institute of Physical and Chemical Research (RIKEN), Hirosawa 2-1, Wako, Saitama 351-0198, Japan*

<sup>2</sup>*Department of Physics, Kyushu University, Fukuoka 812-8581, Japan*

<sup>3</sup>*Department of Physics, Chiba-Keizai College, Inage, Chiba 263-0021, Japan*

(Dated: July 27, 2018)

We accurately analyze the  ${}^6\text{He}+{}^{209}\text{Bi}$  scattering at 19 and 22.5 MeV near the Coulomb barrier energy, using the continuum-discretized coupled-channels method (CDCC) based on the  $n+n+{}^4\text{He}+{}^{209}\text{Bi}$  four-body model. The three-body breakup continuum of  ${}^6\text{He}$  is discretized by diagonalizing the internal Hamiltonian of  ${}^6\text{He}$  in a space spanned by the Gaussian basis functions. The calculated elastic and total reaction cross sections are in good agreement with the experimental data, while the CDCC calculation based on the di-neutron model of  ${}^6\text{He}$ , i.e., the  ${}^2n+{}^4\text{He}+{}^{209}\text{Bi}$  three-body model, does not reproduce the data.

PACS numbers: 21.45.+v, 24.10.Eq, 25.60.-t, 25.70.De

In the recent measurements of  ${}^6\text{He}+{}^{209}\text{Bi}$  scattering at 19 and 22.5 MeV near the Coulomb barrier energy [1, 2], large enhancement of the  $\alpha$ -emission cross section, which dominated the total reaction cross section, compared with that for the corresponding  ${}^6\text{Li}$ -induced reactions was reported. In order to clarify the nature of the enhancement, Keeley *et al.* [3] analyzed the scattering by means of the continuum-discretized coupled-channels method (CDCC) [4, 6, 7] that is a fully quantum-mechanical method for describing scattering of a three-body system. In the analysis, the  ${}^6\text{He}+{}^{209}\text{Bi}$  system was assumed to be the  ${}^2n+{}^4\text{He}+{}^{209}\text{Bi}$  three-body system, that is, the neutron pair in  ${}^6\text{He}$  was treated as a single particle, di-neutron ( ${}^2n$ ). They found that the enhancement of the total reaction cross section of the  ${}^6\text{He}+{}^{209}\text{Bi}$  scattering was due to the electric dipole ( $E1$ ) excitation of  ${}^6\text{He}$  to its continuum states, i.e. Coulomb breakup processes of  ${}^6\text{He}$ , which was approximately absent in the  ${}^6\text{Li}+{}^{209}\text{Bi}$  scattering case. Their calculation, however, did not reproduce the angular distribution of the measured elastic cross section and overestimated the measured total reaction cross section by a factor of three. Thus, reaction mechanisms of the  ${}^6\text{He}+{}^{209}\text{Bi}$  scattering are not fully understood.

In the very recent work [8], it was reported that the elastic cross sections of the  ${}^6\text{He}+{}^{209}\text{Bi}$  scattering calculated within the same framework as in Ref. [3] with the strength of the dipole coupling potentials multiplied by 0.5 reproduced the experimental data. This indicates that the  $E1$  excitation strength of  ${}^6\text{He}$  cannot be accurately reproduced by the  ${}^2n+{}^4\text{He}$  model. Since  ${}^6\text{He}$  is well known as a two-neutron halo nucleus, its structure should be described by the  $n+n+{}^4\text{He}$  three-body system rather than the  ${}^2n+{}^4\text{He}$  two-body one. Thus, it is necessary to analyze the  ${}^6\text{He}+{}^{209}\text{Bi}$  scattering by using the  $n+n+{}^4\text{He}+{}^{209}\text{Bi}$  four-body model. Furthermore, a fully quantum-mechanical method such as CDCC is highly required to analyze the scattering near the Coulomb barrier energies in which both nuclear and Coulomb breakup

processes are significant.

In our previous work [9], we proposed four-body CDCC that is the extension of CDCC and describes four-body breakup processes. In four-body CDCC, the three-body breakup continuum of the projectile is discretized by diagonalizing the internal Hamiltonian in a space spanned by the Gaussian basis functions. So far the Gaussian basis function was used with success for solving bound-state problems of few-body systems. The approach is called the Gaussian expansion method (GEM) [10]. The application of the Gaussian basis function to the discretization of breakup continuum is a natural extension of GEM. In general, the method that describes the breakup continuum by a superposition of  $L^2$ -type basis functions is called the pseudostate method [11], and other basis functions have been also proposed so far [12, 13, 14]. Four-body CDCC was successfully applied to  ${}^6\text{He}+{}^{12}\text{C}$  scattering at 18 and 229.8 MeV in which only nuclear breakup was significant. The elastic and breakup cross sections calculated with four-body CDCC are found to converge as the number of Gaussian basis functions is increased [9]. This indicates that the set of discretized continuum states obtained by the pseudostate method with GEM forms a complete set with good accuracy in a finite region of space that is important for the four-body reaction process concerned. Furthermore, in Ref. [15], applicability of CDCC with the pseudostate method to Coulomb breakup processes, in which large modelspace of the projectile is required because of the long-range property of Coulomb coupling potentials, was shown for the  ${}^8\text{B}+{}^{58}\text{Ni}$  scattering at 25.8 MeV. Thus, it is expected that four-body CDCC with GEM accurately describes the  ${}^6\text{He}+{}^{209}\text{Bi}$  scattering near the Coulomb barrier energy.

In this Rapid Communication, we analyze  ${}^6\text{He}+{}^{209}\text{Bi}$  scattering at 19 and 22.5 MeV by means of four-body CDCC. This is the first application of four-body CDCC to low-energy scattering in which both nuclear and Coulomb breakup processes are significant. We show that four-body CDCC reproduces the measured elastic and total reaction cross sections reasonably well. Effects of four-body breakup processes on the elastic scattering are investigated through the dynamical polariza-

\*Electronic address: taku2scp@rarfaxp.riken.jp

tion (DP) potential. We discuss the reason why the di-neutron model of  ${}^6\text{He}$  is insufficient to describe the  ${}^6\text{He}+{}^{209}\text{Bi}$  scattering.

We assume that the  ${}^6\text{He}+{}^{209}\text{Bi}$  scattering is described as the  $n+n+{}^4\text{He}+{}^{209}\text{Bi}$  four-body system. The model Hamiltonian of the system is defined by

$$H = K_R + U_{n\text{Bi}}(R_{n_1}) + U_{n\text{Bi}}(R_{n_2}) + U_{\alpha\text{Bi}}(R_\alpha) + H_6, \quad (1)$$

where  $\mathbf{R}_X$  ( $\mathbf{R}$ ) is the coordinate of particle  $X$  (the center-of-mass of  ${}^6\text{He}$ ) relative to  ${}^{209}\text{Bi}$ ,  $K_R$  is the kinetic energy associated with  $\mathbf{R}$ , and  $H_6$  is the internal Hamiltonian of  ${}^6\text{He}$ . The potential  $U_{n\text{Bi}}$  ( $U_{\alpha\text{Bi}}$ ) represents the interaction between  $n$  ( ${}^4\text{He}$ ) and  ${}^{209}\text{Bi}$ . It should be noted that  $U_{\alpha\text{Bi}}$  contains a Coulomb part that causes Coulomb breakup processes in the  ${}^6\text{He}+{}^{209}\text{Bi}$  scattering. In four-body CDCC, the total wave function of the four-body system is expanded in terms of a finite number of the internal wave functions of the  ${}^6\text{He}$  projectile. The internal wave functions including the bound and discretized-continuum states are generated with GEM as mentioned above. In GEM, the  $n$  th eigenstate  $\Phi_{nIm}$  of  ${}^6\text{He}$  with the total spin  $I$  and its projection on the  $z$ -axis  $m$  is written as

$$\Phi_{nIm} = \sum_{c=1}^3 \psi_{nIm}^{(c)}(\mathbf{y}_c, \mathbf{r}_c), \quad (2)$$

where  $c$  denotes a set of Jacobi coordinates shown in Fig. 1. Each  $\psi_{nIm}^{(c)}$  is then expanded in terms of the Gaussian basis functions:

$$\begin{aligned} \psi_{nIm}^{(c)}(\mathbf{y}_c, \mathbf{r}_c) = & \sum_{\lambda, \ell, \Lambda, S} \sum_{i=1}^{i_{\max}} \sum_{j=1}^{j_{\max}} A_{i\lambda j\ell\Lambda S}^{(c)nI} \\ & \times y_c^\lambda r_c^\ell e^{-(y_c/\bar{y}_i)^2} e^{-(r_c/\bar{r}_j)^2} \\ & \times \left[ [Y_\lambda(\hat{\mathbf{y}}_c) \otimes Y_\ell(\hat{\mathbf{r}}_c)]_\Lambda \otimes \left[ \eta_{\frac{1}{2}}^{(n_1)} \otimes \eta_{\frac{1}{2}}^{(n_2)} \right]_S \right]_{Im}, \quad (3) \end{aligned}$$

where  $\lambda$  ( $\ell$ ) is the angular momentum regarding the Jacobi coordinate  $\mathbf{y}_c$  ( $\mathbf{r}_c$ ), and  $\eta_{1/2}$  is the spin wave function of each valence neutron ( $n_1$  or  $n_2$ ). In actual calculation we truncate  $\lambda$  and  $\ell$  at appropriate maximum values,  $\lambda_{\max}$  and  $\ell_{\max}$ , respectively. The Gaussian range parameters are taken to lie in geometric progression:

$$\bar{y}_i = \bar{y}_1 (\bar{y}_{\max}/\bar{y}_1)^{(i-1)/(i_{\max}-1)}, \quad (4)$$

$$\bar{r}_j = \bar{r}_1 (\bar{r}_{\max}/\bar{r}_1)^{(j-1)/(j_{\max}-1)}. \quad (5)$$

The eigenstate  $\Phi_{nIm}$  of  ${}^6\text{He}$  is antisymmetrized for the exchange between  $n_1$  and  $n_2$ ; we then have  $A_{i\lambda j\ell\Lambda S}^{(2)nI} = (-)^S A_{i\lambda j\ell\Lambda S}^{(1)nI}$  and  $(-)^{\lambda+S} = 1$  for  $c = 3$ . Meanwhile, the exchange between each valence neutron and each nucleon in  ${}^4\text{He}$  is treated approximately by the orthogonality condition model [16]. The eigenenergies  $\epsilon_{nI}$  of  ${}^6\text{He}$  and the corresponding expansion-coefficients  $A_{i\lambda j\ell\Lambda S}^{(c)nI}$  are determined by diagonalizing  $H_6$  [17, 18].

Using the internal states of  ${}^6\text{He}$  thus obtained, we expand the total wave function of the  $n+n+{}^4\text{He}+{}^{209}\text{Bi}$  four-body system with the total angular momentum  $J$  and its projection on

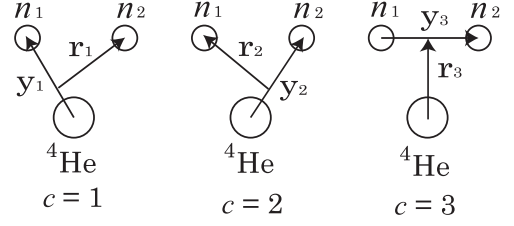


FIG. 1: Jacobi coordinates of the three rearrangement channels ( $c = 1-3$ ) adopted for the  $n+n+{}^4\text{He}$  model of  ${}^6\text{He}$ .

the  $z$ -axis  $M$ ,  $\Psi^{JM}$ :

$$\Psi^{JM} = \sum_{nIL} \chi_{nIL}^J(P_{nI}, R)/R \mathcal{Y}_{nIL}^{JM}, \quad (6)$$

$\mathcal{Y}_\gamma^{JM} = [\Phi_{nI}(\mathbf{y}_c, \mathbf{r}_c) \otimes i^L Y_L(\hat{\mathbf{R}})]_{JM}$  and  $L$  is the orbital angular momentum regarding  $\mathbf{R}$ ; below we denotes the channels  $\{n, I, L\}$  as  $\gamma$ . The expansion-coefficient  $\chi_\gamma^J$  represents the relative motion between the  ${}^6\text{He}$  projectile and the  ${}^{209}\text{Bi}$  target and  $P_{nI}$  is the corresponding relative momentum. Multiplying the four-body Schrödinger equation  $(H - E)\Psi^{JM} = 0$  by  $\mathcal{Y}_\gamma^{JM}$  from the left and integrating over all variables except  $R$ , one obtains the set of coupled differential equations for  $\chi_\gamma^J$

$$\begin{aligned} \left[ \frac{d^2}{dR^2} - \frac{L(L+1)}{R^2} - \frac{2\mu}{\hbar^2} U_{\gamma\gamma}(R) + P_{nI}^2 \right] \chi_\gamma^J(P_{nI}, R) \\ = \frac{2\mu}{\hbar^2} \sum_{\gamma' \neq \gamma} U_{\gamma'\gamma}(R) \chi_{\gamma'}^J(P_{n'I'}, R), \quad (7) \end{aligned}$$

where the coupling potential  $U_{\gamma'\gamma}(R)$  is defined by

$$U_{\gamma'\gamma}(R) = \langle \mathcal{Y}_{\gamma'}^{JM} | U_{n\text{Bi}}(R_{n_1}) + U_{n\text{Bi}}(R_{n_2}) + U_{\alpha\text{Bi}}(R_\alpha) | \mathcal{Y}_\gamma^{JM} \rangle$$

and  $\mu$  is the reduced mass between  ${}^6\text{He}$  and  ${}^{209}\text{Bi}$ . We obtain the elastic and discrete breakup  $S$ -matrix elements by solving Eq. (7) under an appropriate asymptotic boundary condition [4, 19]. Details of the formalism of CDCC are shown in Ref. [4].

TABLE I: The maximum internal angular momenta and the Gaussian range parameters for each Jacobi coordinate.

$c$	$I^\pi$	$\lambda_{\max}$	$\ell_{\max}$	$\bar{y}_1$ [fm]	$\bar{y}_{\max}$ [fm]	$\bar{r}_1$ [fm]	$\bar{r}_{\max}$ [fm]
3	$0^+$	1	1	0.1	15.0	0.5	15.0
1,2	$0^+$	1	1	0.5	15.0	0.5	15.0
3	$1^-$	1	1	0.1	15.0	0.5	15.0
1,2	$1^-$	1	1	0.5	15.0	0.5	15.0
3	$2^+$	2	2	0.1	15.0	0.5	15.0
1,2	$2^+$	1	1	0.5	15.0	0.5	15.0

In the present four-body CDCC calculation for  ${}^6\text{He}+{}^{209}\text{Bi}$  scattering at 19 and 22.5 MeV, we take  $I^\pi = 0^+, 1^-,$  and  $2^+$  states for  ${}^6\text{He}$ . Inclusion of  $1^-$  state is essential to describe Coulomb breakup processes. As for the internal Hamiltonian

of  ${}^6\text{He}$ , we adopt the same Hamiltonian as used in Ref. [9]. We show in Table I the maximum values of the internal angular momenta,  $\lambda_{\text{max}}$  and  $\ell_{\text{max}}$ , and the Gaussian range parameters,  $\bar{y}_1$ ,  $\bar{y}_{\text{max}}$ ,  $\bar{r}_1$ , and  $\bar{r}_{\text{max}}$ , used in the calculation of  $\Phi_{nIm}$ . For each set of  $\{c, \lambda, \ell, \Lambda, S\}$ , we take  $i_{\text{max}} = j_{\text{max}} = 10$ . These values of the parameters are found to give good convergence of the calculated elastic and total reaction cross sections. It should be noted that the maximum value of each Gaussian range parameter is 15 fm, which is quite larger than that used in the four-body CDCC analysis of  ${}^6\text{He}$  nuclear breakup [9], i.e. 10 fm. Some parameters shown in Table I depend on  $I^\pi$  and  $c$ , while in Eqs. (3)–(5) the dependence has not been shown for simplicity.

We select the  $\Phi_{nIm}$  with  $\epsilon_{nI} \leq 7$  MeV among those obtained by diagonalizing  $H_6$  and use them in actual CDCC calculation, since the  $\Phi_{nIm}$  with  $\epsilon_{nI} > 7$  MeV are found to have no effect on the calculated cross sections of the  ${}^6\text{He}+{}^{209}\text{Bi}$  scattering shown below. The resulting number of the discrete states for the  $0^+$ ,  $1^-$ , and  $2^+$  states is 37 (including the ground state of  ${}^6\text{He}$ ), 44, and 53, respectively. As for the nuclear parts of  $U_{n\text{Bi}}$  and  $U_{\alpha\text{Bi}}$ , respectively, we take the optical potentials of Koning and Delaroche [20] and of Barnett and Lilley [21]. The maximum value of  $L$  is taken to be 200 and the scattering wave function  $\chi_\gamma^J$  is connected to its appropriate asymptotic form at  $R = 200$  fm.

Below we show also results of CDCC calculation based on the  ${}^2n+{}^4\text{He}+{}^{209}\text{Bi}$  three-body model to see three-body breakup effects on the elastic and total reaction cross sections. In this model the di-neutron ( ${}^2n$ ) model of  ${}^6\text{He}$  is used and the intrinsic spin and the relative energy of  ${}^2n$  are assumed to be zero. We henceforth call CDCC based on the model above three-body CDCC. As for the interaction between  ${}^2n$  and  ${}^4\text{He}$ , we take the same parameter as used in Ref. [3]. The  ${}^2n+{}^4\text{He}$  continuum is discretized by the pseudostate method described in Ref. [11] and truncated at the relative momentum  $k = 0.7 \text{ fm}^{-1}$  that corresponds to about 7 MeV of the excitation energy of  ${}^6\text{He}$ . The number of the discrete state is 9 for each of the  $0^+$ ,  $1^-$ , and  $2^+$  states of  ${}^6\text{He}$ . The range parameters of the Gaussian basis functions are  $(a_1 = 0.5 \text{ fm}, a_{n_a} = 20.0 \text{ fm}, n_a = 20)$  with the same notation as in Ref. [11]. We adopt the optical potential of Barnett and Lilley [21] for the nuclear part of  $U_{\alpha\text{Bi}}$ , as in the four-body CDCC calculation, and the  $d-{}^{208}\text{Pb}$  (type-a) optical potential at the deuteron incident energy of 15.0 MeV [22] for the interaction between  ${}^2n$  and  ${}^{209}\text{Bi}$ . Other parameters of the modelspace are the same as in the four-body CDCC calculation.

Figure 2 shows the angular distribution of the elastic differential cross section for the  ${}^6\text{He}+{}^{209}\text{Bi}$  scattering at 19 MeV. The solid line is the result of four-body CDCC and the dashed line is that of three-body CDCC. The results of four-body CDCC and three-body CDCC without breakup effects of  ${}^6\text{He}$  are shown by the dotted and dot-dashed lines, respectively. The difference between the solid and dotted (dashed and dot-dashed) lines shows effects of the four-body (three-body) breakup on the elastic cross section. One sees that four-body CDCC reproduces the experimental data well, while three-body CDCC underestimates the data at middle angles of  $50^\circ$ –

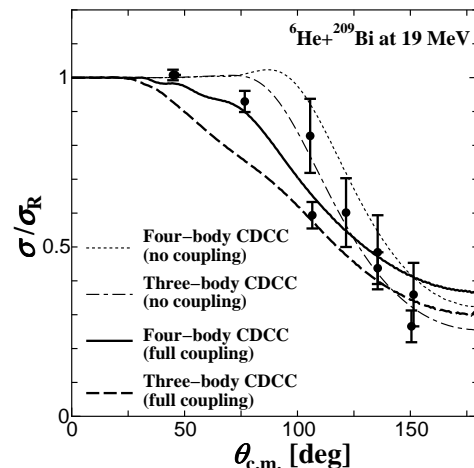


FIG. 2: Angular distribution of the elastic differential cross section as the ratio to the Rutherford cross section for the  ${}^6\text{He}+{}^{209}\text{Bi}$  scattering at 19 MeV. The solid (dashed) and dotted (dot-dashed) lines show the results of the four-body CDCC (three-body CDCC) calculation with and without breakup effects, respectively. The experimental data are taken from Ref. [1, 2]. The incident energy for the experimental data in the laboratory frame is shown to be 19 MeV and 18.4 MeV in the first [1] and second [2] papers of Aguilera *et al.*, respectively; in the present study we take 19 MeV.

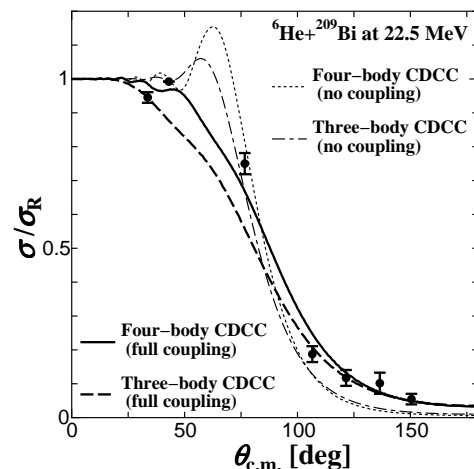


FIG. 3: The same as in Fig. 2 but for  ${}^6\text{He}+{}^{209}\text{Bi}$  scattering at 22.5 MeV. The experimental data are taken from Ref. [1, 2]. We take the incident energy of 22.5 MeV shown in the first paper of Aguilera *et al.* [1].

$100^\circ$ . The dashed line is consistent with the result of Ref. [3]; it should be noted that the real part of each coupling potential was multiplied by 0.8 in Ref. [3], while in the present study such a renormalization factor is not included. Figure 3 shows the result at 22.5 MeV and features of the result are just the same as at 19 MeV.

We show in Fig. 4 the calculated total reaction cross sections; the solid (open) circles represent the results of four-body (three-body) CDCC. The open squares are the experimental values of the  $\alpha$ -emission cross sections [1] added by

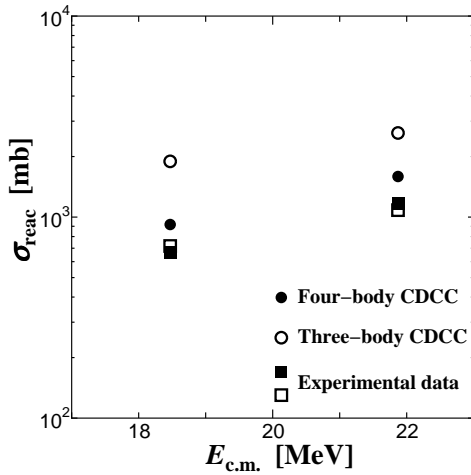


FIG. 4: Total reaction cross sections of  ${}^6\text{He}+{}^{209}\text{Bi}$  scattering as a function of the incident energy in the center of mass frame. The four values on the left (right) side correspond to the  ${}^6\text{He}$  incident energy of 19 MeV (22.5 MeV) in the laboratory frame. The solid and open circles represent the results of the four-body CDCC calculation and the three-body CDCC calculation, respectively. The experimental data shown by the open and solid squares are taken from Ref. [1]; see the text for details.

the fusion cross sections [23], while the solid squares are the total reaction cross sections evaluated from an optical-model analysis of the measured elastic cross sections [1]. The figure shows that three-body CDCC overestimates the experimental data by a factor of about three. This overestimation is consistent with the fact that three-body CDCC underestimates the elastic cross section as shown in Figs. 2 and 3. On the contrary, four-body CDCC reproduces the experimental data quite well, which shows the importance of the accurate description of three-body breakup continuum of  ${}^6\text{He}$ . The remaining difference of about a few tens of % between the results of four-body CDCC and the data needs further investigation, including analysis of  ${}^6\text{He}+{}^{208}\text{Pb}$  scattering in barrier-energy region [24].

In order to clarify the reason why the total reaction cross section calculated with three-body CDCC is much larger than that with four-body CDCC, we see first the strength of E1 transition based on the two models. The non-energy weighted E1 excitation strength  $B(E1)$  from the ground state  $\Phi_{000}$  of  ${}^6\text{He}$  to its excited states  $\Phi_{n1m}$  with  $I = 1$  is given by

$$B(E1) = \left(\frac{2}{3}\right)^2 \sum_n \sum_{\mu, m} |\langle \Phi_{n1m} | y_3 Y_{1\mu}(\hat{y}_3) | \Phi_{000} \rangle|^2. \quad (8)$$

The summation over  $n$  is taken up to a value that corresponds to the excitation energy of  ${}^6\text{He}$  of 7 MeV, i.e. the maximum energy of the modelspace of the present analysis. The resulting values of  $B(E1)$  based on the  ${}^2n+{}^4\text{He}$  model and the  $n+n+{}^4\text{He}$  model are, respectively,  $1.5 e^2\text{fm}^2$  and  $0.9 e^2\text{fm}^2$ . The latter agrees well with the experimental value reported by Aumann *et al.* [25], which is consistent with the conclusion in Ref. [26]. Thus, the E1 strength is overestimated in the di-neutron model. This indicates that the di-neutron model

overshoots the breakup cross section of the  ${}^6\text{He}+{}^{209}\text{Bi}$  scattering, which is the main reason why three-body CDCC overestimates the result of four-body CDCC, hence the measured total reaction cross section. This conclusion is qualitatively consistent with that drawn in Ref. [8], in which, as mentioned above, three-body CDCC with the strength of the dipole coupling potentials multiplied by 0.5 was shown to reproduce the elastic scattering data of the  ${}^6\text{He}+{}^{209}\text{Bi}$  scattering.

Next we discuss the difference of the optical potentials taken in the  ${}^2n+{}^4\text{He}+{}^{209}\text{Bi}$  three-body model and the  $n+n+{}^4\text{He}+{}^{209}\text{Bi}$  four-body model. As one sees in Figs. 2 and 3, the elastic cross section without breakup effects calculated with the three-body model underestimates that with the four-body model. This means that the diagonal component of the imaginary potential in the elastic channel based on the three-body model is deeper than that on the four-body model. Thus, the three-body model yields an absorption cross section larger than the four-body model does. This is also an important factor for the enhancement of the total reaction cross section calculated with three-body CDCC.

Finally, we see the difference between three-body CDCC and four-body CDCC in more detail by evaluating the dynamical polarization (DP) potential  $U_{\text{DP}}^J$  and the equivalent local potential  $U_{\text{eq}}^J(R)$ . Explicit form of the two potentials is given by

$$U_{\text{DP}}^J(R) = \frac{\sum_{\gamma \neq \gamma_0} U_{\gamma\gamma_0}(R) \chi_{\gamma}^J(P_{nI}, R)}{\chi_{\gamma_0}^J(P_{0I_0}, R)} \quad (9)$$

and

$$U_{\text{eq}}^J(R) \equiv U_{\text{DP}}^J(R) + U_{\gamma_0\gamma_0}(R),$$

where the subscript 0 denotes the incident channel.

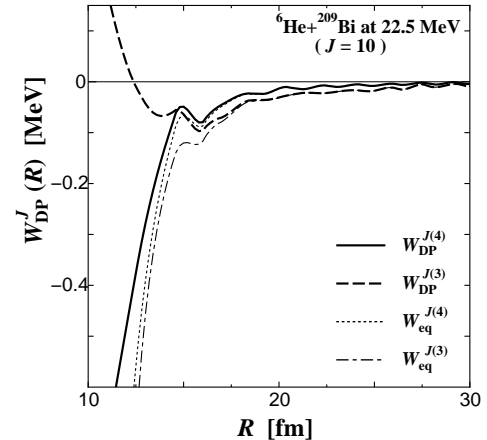


FIG. 5: The imaginary parts of the dynamical polarization (DP) potential and the equivalent local potential for the  ${}^6\text{He}+{}^{209}\text{Bi}$  scattering at 22.5 MeV with  $J = 10$ . The solid and dotted lines, respectively, represent the results of the DP and equivalent local potential calculated with four-body CDCC. The dashed and dotted-dash lines correspond to those calculated with three-body CDCC based on the di-neutron model of  ${}^6\text{He}$ .

Figure 5 shows the imaginary parts  $W_{\text{DP}}^{J(4)}$  and  $W_{\text{DP}}^{J(3)}$  of  $U_{\text{DP}}^J$  calculated with four-body CDCC (solid line) and three-

body CDCC (dashed line), respectively, for the  ${}^6\text{He}+{}^{209}\text{Bi}$  scattering at 22.5 MeV. Also shown are the results of the imaginary parts of  $U_{\text{eq}}^J$  calculated with four-body and three-body CDCC, i.e.  $W_{\text{eq}}^{J(4)}$  and  $W_{\text{eq}}^{J(3)}$ . It should be noted that the figure shows the potentials only in the peripheral region, i.e.,  $10 \text{ fm} \leq R \leq 30 \text{ fm}$ , where the scattering wave has nonnegligible values. The results correspond to  $J = 10$  at which the partial reaction cross section becomes maximum. It is confirmed that the DP potential hardly depends on  $J$  around  $J = 10$  in the peripheral region shown in Fig. 5. It should be noted that  $U_{\text{DP}}^J$  defined by Eq. (9), or  $U_{\text{eq}}^J(R)$ , is not a smooth function since it is divided by the oscillating function  $\chi_{\gamma_0}^J$ . Each line in Fig. 5 is obtained by interpolation of  $U_{\text{DP}}^J(R)$  (or  $U_{\text{eq}}^J(R)$ ) at  $R$  where  $|\chi_{\gamma_0}^J|$  is more than 90% of its maximum value in the asymptotic region; this simple way of evaluating  $U_{\text{DP}}^J(R)$  and  $U_{\text{eq}}^J(R)$  is appropriate for the present purpose. The  $S$ -matrix element calculated with the interpolated DP potential reproduces the one obtained by CDCC within the relative error of 3%.

One sees from Fig. 5 that both  $W_{\text{DP}}^{J(3)}$  and  $W_{\text{DP}}^{J(4)}$  have a long ranged tail, which is induced by Coulomb breakup processes. In the tail region of  $R \geq 15 \text{ fm}$ , where the imaginary part of  $U_{\gamma_0\gamma_0}$  is negligible and  $W_{\text{DP}}^J$  agrees with  $W_{\text{eq}}^J$ ,  $W_{\text{DP}}^{J(3)}$  is deeper than  $W_{\text{DP}}^{J(4)}$ . This is consistent with the fact mentioned above that the strength of E1 transition is overestimated by the di-neutron model of  ${}^6\text{He}$ , which is used in the three-body CDCC calculation. On the other hand,  $W_{\text{DP}}^{J(3)}$  is shallower than  $W_{\text{DP}}^{J(4)}$  in the region of  $R \leq 15 \text{ fm}$ . However, the imaginary part of  $U_{\gamma_0\gamma_0}$  calculated with three-body CDCC is, as mentioned above, much deeper than that with four-body CDCC, which makes  $W_{\text{eq}}^{J(3)}$  deeper than  $W_{\text{eq}}^{J(4)}$  in this region. Thus, the imaginary part of the equivalent local potential, which dictates the total reaction cross section, calculated with three-body CDCC is deeper than that with four-body CDCC in the entire region that is important for the  ${}^6\text{He}+{}^{209}\text{Bi}$  scattering concerned. This conclusion is consistent with the discussion above and the result shown in Fig. 4.

The real part  $V_{\text{DP}}^J$  of the DP potential also plays important roles in the  ${}^6\text{He}+{}^{209}\text{Bi}$  scattering. It is found that  $V_{\text{DP}}^J$

is repulsive for  $R \leq 15 \text{ fm}$ , where nuclear breakup processes are significant, and attractive for  $R \geq 15 \text{ fm}$ , where Coulomb breakup processes are dominant. The difference between  $V_{\text{DP}}^J$  calculated with three-body CDCC and four-body CDCC in the outer region is just the same as for  $W_{\text{DP}}^J$  shown in Fig. 5.

In summary, the  ${}^6\text{He}+{}^{209}\text{Bi}$  scattering at 19 MeV and 22.5 MeV, near the Coulomb barrier energy, is analyzed with the continuum-discretized coupled-channels method (CDCC) based on the  $n+n+{}^4\text{He}+{}^{209}\text{Bi}$  four-body model, four-body CDCC, that treats both nuclear and Coulomb breakup processes simultaneously. It is found that the angular distribution of the elastic cross section and the total reaction cross section calculated with four-body CDCC reasonably reproduce the experimental data with no free adjustable parameter. Three-body CDCC based on the  ${}^2n+{}^4\text{He}+{}^{209}\text{Bi}$  three-body model, i.e. di-neutron model of  ${}^6\text{He}$ , turns out to overestimate the total reaction cross section by a factor of about three, which is consistent with the conclusion of the previous work of Keeley *et al.* [3]. The value of  $B(E1)$  calculated by the di-neutron model overestimates the experimental one, while the  $n+n+{}^4\text{He}$  three-body model reproduces the data well, as pointed out in Ref. [8]. This makes the imaginary part of the dynamical polarization potential calculated with three-body CDCC deeper than that with four-body CDCC in the tail region. Also important fact is that three-body CDCC contains a deep imaginary part of the diagonal potential for the elastic channel compared with four-body CDCC does. We thus conclude that the di-neutron model is inadequate to treat breakup continuum of  ${}^6\text{He}$  precisely and a  $n+n+{}^4\text{He}+{}^{209}\text{Bi}$  four-body reaction model is necessary to accurately describe the  ${}^6\text{He}+{}^{209}\text{Bi}$  scattering. Four-body CDCC is indispensable to analyze low energy  ${}^6\text{He}$  scattering in which both nuclear and Coulomb breakup processes are significant.

The authors would like to thank E. Hiyama for helpful discussions on the GEM calculation. T. M. is grateful for financial assistance from the Special Postdoctoral Researchers Program of RIKEN. This work has been supported in part by the Grants-in-Aid for Scientific Research of Monbukagakusyo of Japan and JSPS.

- 
- [1] E. F. Aguilera *et al.*, Phys. Rev. Lett. **84**, 5058 (2000).  
 [2] E. F. Aguilera *et al.*, Phys. Rev. C **63**, 061603(R) (2001).  
 [3] N. Keeley *et al.*, Phys. Rev. C **68**, 054601 (2003).  
 [4] M. Kamimura *et al.*, Prog. Theor. Phys. Suppl. **89**, 1 (1986).  
 [5] N. Austern *et al.*, Phys. Rev. Lett. **63**, 2649 (1989); Phys. Rev. C **53**, 314 (1996).  
 [6] N. Austern *et al.*, Phys. Reports. **154**, 125 (1987).  
 [7] Y. Sakuragi, Phys. Rev. C **35**, 2161 (1987).  
 [8] K. Rusek *et al.*, Phys. Rev. C **72**, 037603 (2005).  
 [9] T. Matsumoto *et al.*, Phys. Rev. C **70**, 061601(R) (2004).  
 [10] For a review, E. Hiyama *et al.*, Prog. Part. Nucl. Phys. **51**, 223 (2003).  
 [11] T. Matsumoto *et al.*, Phys. Rev. C **68**, 064607 (2003).  
 [12] R. Y. Rasoanaivo and G. H. Rawitscher, Phys. Rev. C **39**, 1709 (1989).  
 [13] A. M. Moro *et al.*, Phys. Rev. C **65**, 011602(R) (2002).  
 [14] M. Rodríguez-Gallardo *et al.*, Phys. Rev. C **72**, 024007 (2005).  
 [15] T. Egami *et al.*, Phys. Rev. C **70**, 047604 (2004).  
 [16] S. Saito, Prog. Theor. Phys. **41**, 705 (1969).  
 [17] S. Funada *et al.*, Nucl. Phys. **A575**, 93 (1994).  
 [18] E. Hiyama and M. Kamimura, Nucl. Phys. **A588**, 35 (1995).  
 [19] R. A. D. Piyadasa *et al.*, Phys. Rev. C **60**, 044611 (1999).  
 [20] A. J. Koning and J. P. Delaroche, Nucl. Phys. **A713**, 231 (2003).  
 [21] A. R. Barnett and J. S. Lilley, Phys. Rev. C **9**, 2010 (1974).  
 [22] C. M. Perey and F. G. Perey, Phys. Rev. **132**, 755 (1963).  
 [23] J. J. Kolata *et al.*, Phys. Rev. Lett. **81**, 4580 (1998).  
 [24] K. Rusek *et al.*, Phys. Rev. C **67**, 041604(R) (2003).  
 [25] T. Aumann *et al.*, Phys. Rev. C **59**, 1252 (1999).  
 [26] I. J. Thompson *et al.*, Phys. Rev. C **61**, 024318 (2000).